Three-dimensional light focusing in inverse opal photonic crystals

Kun Ren,[1] Zhi-Yuan Li,[1,*] XiaoBin Ren,[2] Shuai Feng,[1] Bingying Cheng,[1] and Daozhong Zhang[1]
[1]*Beijing National Laboratory for Condensed Matter Physics, Institute of Physics, Chinese Academy of Sciences, Beijing 100080, China*
[2]*School of Physics Science and Information Technology, Liaocheng University, Liaocheng 252059 China and Department of Physics, Beijing Normal University, Beijing 100875, China*

(Received 30 April 2006; revised manuscript received 16 January 2007; published 8 March 2007)

In this paper, we study negative refraction of electromagnetic waves in three-dimensional (3D) inverse opal photonic crystals (PCs). We employ the plane-wave expansion method to calculate the equifrequency surface of the PC structure, from which the frequency window where negative refraction might occur can be determined. We then investigate the propagation of electromagnetic waves radiating from a point source through a flat PC slab by means of a finite-difference time-domain method. We find that wave focusing can be achieved in such a 3D inverse opal PC structure at the negative-refraction frequency window. Because the inverse opal photonic crystal can be routinely synthesized in the optical regime by means of the self-assembly approach, our study opens a way for realization and application of 3D negative-refraction superlenses in the visible and infrared regimes.

DOI: 10.1103/PhysRevB.75.115108 PACS number(s): 78.20.Ci, 42.70.Qs, 41.20.Jb

I. INTRODUCTION

Materials possessing negative index of refraction (NIR) have drawn rapidly growing interests in recent years due to their novel properties and promising applications. It has been suggested that a parallel-sided slab made of NIR materials can focus electromagnetic (EM) waves just like a lens. Negative index materials (NIMs), which are also known as left-handed materials (LHMs), were first introduced by Veselago in 1960s.[1] However, this subject remained dormant for more than 30 years because there are no naturally occurring materials whose permittivity ε and permeability μ are negative simultaneously. It is the pioneering work of Pendry *et al.* that opens the door to design left-handed materials.[2,3] He also proposed superlens with image below the classical diffraction limit.[4] The first experiment[5] was conducted and demonstrated by using a metamaterial composed of a three-dimensional array of copper wires and split ring resonators to provide negative permittivity ε and negative permeability μ, respectively. The amazing potential of NIR-based lenses[4] evoked an upsurge to develop other new materials that can exhibit this unique property. It is found that negative refraction can occur at an interface associated with a uniaxial anisotropic medium with only one of the four parameters of ε and μ tensors being negative.[6,7] Zhang *et al.* have recently found and demonstrated experimentally that negative refraction can be realized even without any component of the ε or μ tensor being negative.[8]

Another way to achieve negative refraction is by photonic crystals (PCs), or even by photonic quasicrystals.[9] Negative refraction in PCs possesses several merits. For example, compared with LHM, PCs have much smaller losses even at optical frequency because a nonconducting dielectric material is used. Negative refraction based on PCs has been studied extensively. There have been a large number of theoretical studies[10–19] and a variety of experimental demonstrations on this subject.[20–24] It has been found that negative refraction can occur for several reasons in PCs (Ref. 25) and is not always associated with the negative refraction occurring at the interface of a homogeneous medium with $n=-1$. In one mechanism,[11,20] the refractive index is actually positive and the negative refraction is based on the anisotropic shape of the equifrequency surfaces (EFSs). It was found that in this case such superlensing is a near-field phenomenon[12] and a result of the interplay between negative refraction and surface waves.[13] Another mechanism is left-handed behavior,[14–16,22] which relies on a material slab with an effective negative refractive index. A manifestation of lensing based on negative refraction with $n=-1$ is the geometric-optics rule for the location of object and image point.[15] Negative refraction in near-infrared wavelengths has been investigated experimentally in GaAs-based PCs (Ref. 26) and in Si-polyimide PC membranes.[27]

The full realization of a perfect lens and other applications of negative refraction, in principle, desire the fabrication of three-dimensional, homogeneous, isotropic left-handed materials.[1] Fairly speaking, this is, while fundamental, a difficult and challenging task. Until now, most research efforts focus on two-dimensional (2D) periodic structures where negative refraction can occur in a wide variety of lattice structures and for different polarizations. These 2D flat lenses have limitations on realistic applications. Moreover, compact optical circuits have an appeal to achieve negative refraction superlens imaging in the optical and near-infrared spectrum windows. Thus, it is necessary to design three-dimensional (3D) structures that enable fully 3D negative refraction in the optical regime. Different from the 2D cases, 3D negative refraction does not depend on the polarization of the object source light. To date, studies on 3D negative refraction in PCs are still very few[16,28–31] and the corresponding experiments are conducted mainly in the microwave regime. The designed PC structures are very difficult to realize in the optical regime. Ao and He recently presented a design of a complex 3D NIR PC based on the interference lithography.[16] However, the interference lithography technique is only efficient for polymer structure, and the synthesis of a high refractive index contrast structure such as a germanium PC as investigated in Ref. 16 from the polymer template has been subject to numerous substantial

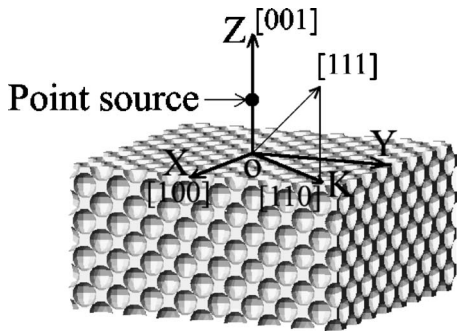

FIG. 1. Schematic diagram of a PC slab lens made from an array of air spheres. The PC slab is ten layers of air spheres thick in the z direction and 30 layers of air spheres wide in both the x and y directions. A point source is located on top of the slab.

technical obstacles. Until now no successful report has been made.

The situation suggests that we should pay more attention to the 3D PC structures that have been successfully fabricated in the visible and near-infrared wavelength regimes. A typical example is the inverse opal photonic crystal.[32–35] After extensive exploration of the chemical self-assembly technique in the last decade, such photonic crystals can be readily synthesized with the lattice constant ranging from visible to infrared wavelengths. In this paper, we will investigate the optical properties of this 3D system and see whether negative refraction can occur in this kind of PC structures. We will first look at the dispersion diagram and EFS of the crystal, from which the propagation behavior of light can be quantitatively understood and roughly predicted. We will then investigate the propagation of light from a point source across a flat slab of the inverse opal photonic crystal, from which the focusing behavior of the crystal can be clearly inferred.

II. BAND DIAGRAM AND EFS CONTOUR ANALYSIS

The inverse opal structure we study consists of periodic air spheres embedded in a dielectric background with permittivity $\varepsilon=12.25$ (i.e., Si inverse opal). These air spheres are arranged in a close-packed face-centered-cubic (fcc) lattice with a filling ratio $f=0.74$. The schematic diagram of the slab lens is depicted in Fig. 1. The $(1\bar{1}0)$ plane makes an angle of 45° with the yoz plane, and is explicitly plotted in Fig. 1. A good way to study qualitatively and quantitatively the electromagnetic wave beam propagation in the PC is to analyze the wave-vector diagram or equifrequency surface of this PC, whose gradient vector gives the group-velocity vector. The band structure of the 3D PC is much more complicated than that of their 2D counterparts. The plane-wave expansion method[36,37] (PWEM) has been used to obtain the band diagram and EFS, in which Bloch waves are expanded approximately by $9\times9\times9$ plane waves. The frequency is normalized as $\omega a/2\pi c$ (a is the period of the fcc lattice and c is the light speed in vacuum). Figure 2 shows the photonic band structure of this inverse opal PC. Note that the dispersion curve at the third band has a negative slope around the Γ

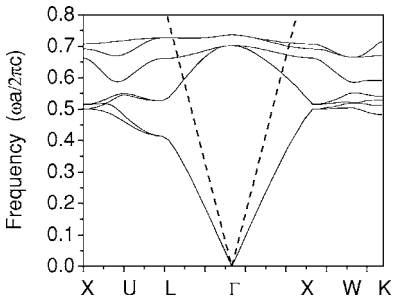

FIG. 2. Photonic band structures for the inverse opal photonic crystal with the background permittivity $\varepsilon=12.25$ and filling ratio $f=0.74$. The dashed line represents the light line for waves in air.

point, which makes it possible to have a negative refraction index in this frequency range. In this region, the third and fourth bands are almost degenerate. We will pay special attention to this frequency band. For a certain frequency in the region where the third band lies, there are also modes from higher bands (the fifth band) along certain symmetry directions. In this paper, the contributions from these modes are not considered. Figure 3(a) presents the cross section of the third-band EFS for waves propagating in the (010) plane with $k_y=0$, namely, the xoz plane at some frequencies of the third band in the first Brillouin zone. The EFS contours shrink with increasing frequencies, and as a result, the group velocity is opposite to the phase velocity for EM waves at

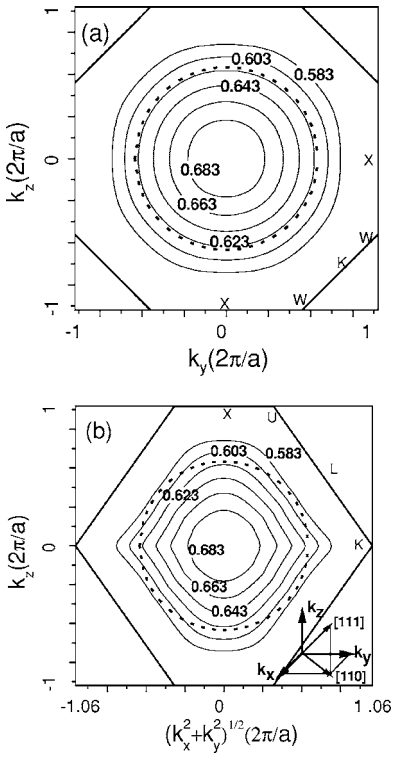

FIG. 3. EFS contours at several frequencies of the third band drawn within the first Brillouin zone in (a) the (010) plane and (b) the $(1\bar{1}0)$ plane, as shown in the inset. The dotted circle is the EFS contour of light in air at $\omega=0.603(2\pi c/a)$. The numbers denote the frequencies in the unit of $2\pi c/a$. The high symmetry points at the boundary of the first Brillouin zone are explicitly noticed.

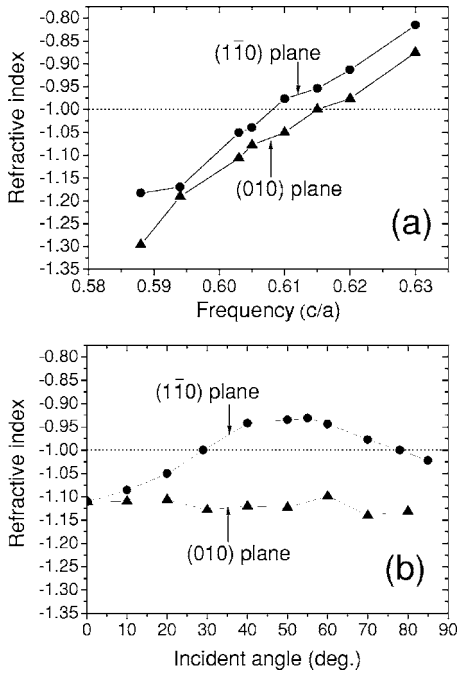

FIG. 4. (a) The effective refractive index n_{eff} vs the frequency in the third band. (b) The effective refractive index n_{eff} vs the incident angle at frequency $\omega=0.603(2\pi c/a)$. The dash-triangle curve is for the (010) plane and the dash-circle curve is for the (1$\bar{1}$0) plane. The dotted lines mark the position of the refractive index of −1.

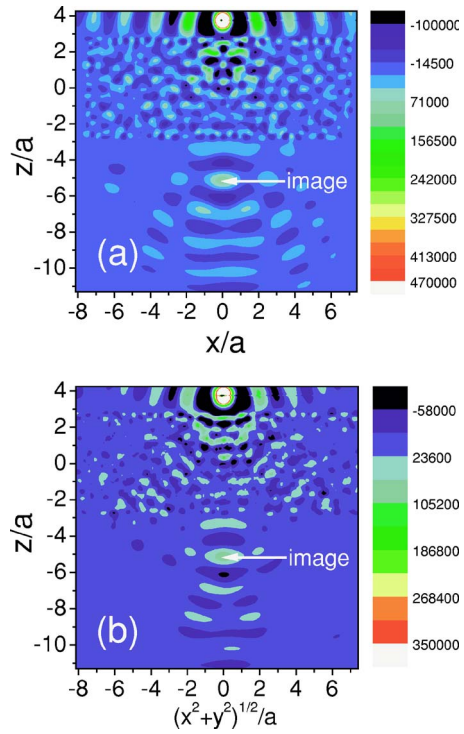

FIG. 5. (Color online) Amplitude distribution of E_y along (a) the vertical xoz plane and (b) the (1$\bar{1}$0) plane. The point source is resonant at $\omega=0.603(2\pi c/a)$ and located at $1.0a$ away from the front surface of the ten-layer-thick slab.

this band. This indicates the possibility of negative refraction at the interface between the PC and air.[10] The wave vector of the excited refraction wave mode (which is located on the EFS) is determined by making the tangential components of wave vectors on both sides of the interface equal. Propagation of EM waves through the PC is then described by using the 3D dispersion relations. In addition, the EFS contours in this plane are very close to perfect circles. The effective refractive index n_{eff} can be obtained from the corresponding EFS contour. This effective index gives the phase velocity of the refracted wave for a certain angle and is, in general, a function of this angle. For the specific case where EFSs are isotropic and the conditions for single beam propagation are satisfied,[25] this value of n_{eff} can be used in Snell's law to provide the angle of the refracted signal. In general, the latter is not in the same direction as the refracted phase velocity. Figure 4(a) shows n_{eff} as a function of the frequency of the incident wave at the 20° incident angle, which is marked by a dash-triangle curve. The effective refractive index $n_{eff}\approx -1$ of PC is found to occur at a frequency around 0.615 (in the unit of normalized frequency $2\pi c/a$). We have $n_{eff}\leqslant -1$ in the frequency region above 0.615, and $-1<n_{eff}<0$ in the frequency region below 0.615.

To fully reflect the 3D propagation behavior of EM waves within the inverse opal PC, we have considered the EFS contours in other orientational planes at the same frequency band within the first Brillouin zone. Figure 3(b) displays the cross section of the third-band EFS in the (1$\bar{1}$0) plane, which contains the wave propagation directions as [001], [111], and [110]. It is clear that the EFS contours in this plane are not circles any more. The variation of the effective refractive index n_{eff} versus the frequency of the incident wave in this (1$\bar{1}$0) plane is also shown in Fig. 4(a) by a dash-circle curve. The anisotropy observed in the n_{eff} index is expected to cause some small deviation in the direction of the refracted beam from the value predicted from Snell's law. In this paper, we choose $\omega=0.603(2\pi c/a)$ as our operating frequency as the negative refraction properties of the crystal appear to be optimum at this frequency. We have retrieved the effective refractive indices for various incident angles at this fixed frequency, and the results are displayed in Fig. 4(b) for wave propagating within the above two crystalline planes. The effective refraction index in the (010) plane keeps nearly equal, which results from the circle EFS contour. As a comparison, the refraction index shows much larger dispersion in the (1$\bar{1}$0) plane due to the remarkable aberration of the EFS contour from an isotropic circle. Within the considered window of incident angle, the refractive index ranges from −0.93 to −1.09.

III. DESIGN OF PC SLAB LENS AND SIMULATION OF THE FOCUSING PROPERTIES

Negative refraction enables the possibility that the flat slab can focus EM wave emerging from an omnidirectional source. When an object is placed at one side of the flat slab, we expect that an image can be observed at the other side. In order to check our analysis, we perform numerical simulations to investigate focus properties of a proposed inverse opal PC structure. The interfaces of the PC slab are cut such

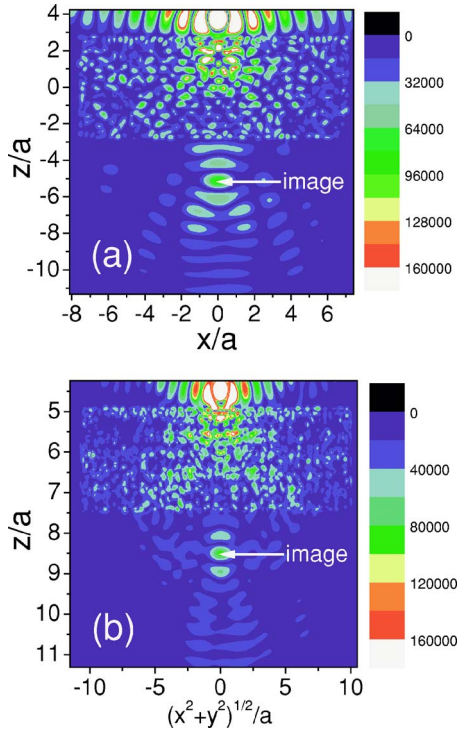

FIG. 6. (Color online) Amplitude magnitude patterns of the total electric field along (a) the vertical *xoz* plane and (b) the $(1\bar{1}0)$ plane. The point source is resonant at $\omega=0.603(2\pi c/a)$ and located at $1.0a$ away from the front surface of the ten-layer-thick slab.

that the surface normal of the slab is parallel to the $\langle 001 \rangle$ direction. The PC slab is ten-layers of air spheres thick in the z direction and 30 layers of air spheres wide in both the x and y directions. A dipole point source is located on top of the slab and the wave propagates along the z axis.

Finite-difference time-domain (FDTD) method[38] is employed with perfectly matched layer (PML) boundary condition[39] to envision how the wave propagates across the PC slab. In the simulation, a continuous wave point source is placed at a distance of $1.0a$ away from the top surface of the PC slab. The source is polarized along the y-axis direction. The wave propagation is probed by looking closely at the field patterns across the slab along different directions and at several parallel observation planes at the other side of the slab. The simulated field distribution along two vertical planes passing through the source is shown in Fig. 5. Figure 5(a) depicts the E_y field pattern along the vertical plane *xoz*. Obviously, one can see a very bright point located below the lower surface of the slab, and its intensity is higher than the surrounding area. The simulation clearly indicates a focusing phenomenon when light wave travels through the slab. The strong intensity point is identified to be the image spot of the point source against the PC slab lens, and it is clearly marked with an arrow in Fig. 5(a). The image spot is located at $2.26a$ away from the back surface of the slab. Note that the image distance plus the objective distance is smaller than the thickness of the PC slab. Therefore, the distance of the image differs from the geometric-optics expectation. However, further simulations reveal that the image distance changes with the source-slab distance. As a result, the object-image distance remains nearly constant. Many factors can influence focusing. The value of the refractive index inside the structure, the impedance that might give reflection at the interface, and the surface termination of the structure might all play a role.[40] However, in our case the deviation from geometric optics is most likely induced by the anisotropy in the EFS, which leads to the deviation from Snell's law. The poor impedance matching and the presence of multiple scattering effect can influence the focusing quality of the PC slab. The field pattern along the *yoz* plane through the source is also simulated, and the result (data not shown here) is the same as for the *xoz* plane because of the crystalline symmetry between these two planes. The calculated field pattern along the $(1\bar{1}0)$ vertical plane is shown in Fig. 5(b). Although it is somewhat different from the field pattern in Fig. 5(a) in the detailed configuration, a focus point (marked by an arrow) can also be found to form on the opposite side of this slab. This means that the focusing also takes place for the wave propagating along the $(1\bar{1}0)$ plane.

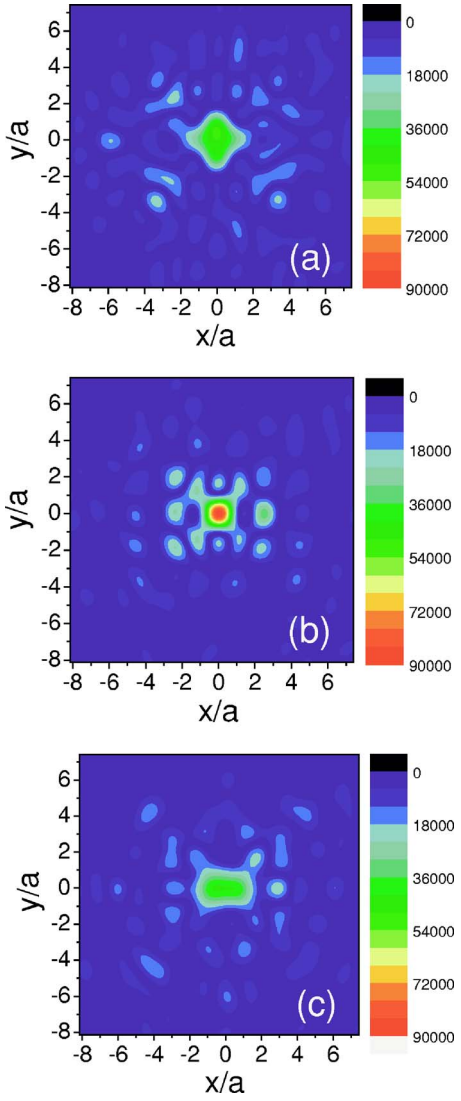

FIG. 7. (Color online) Amplitude distribution of E_y in the horizontal plane *xoy* at different positions: (a) $1.48a$, (b) $2.26a$, and (c) $3.04a$ from the back surface of the slab along the z axis.

In the above, we only consider the E_y field propagation, which is at the same polarization as the light source. As the PC slab is a 3D structure, the complex 3D scattering effect will modify the polarization of the incident wave. In our simulation, we have found that the transmission field involves all three components, namely, E_x, E_y, and E_z. This means that the 3D scattering effect by the complex 3D PC slab can lead to a coupling effect between different polarization states of light. Note that the E_x and E_z wave components do not exhibit an apparent focusing behavior as the E_y component does. However, the E_y field component overwhelms the other two field components and dominates the total electric field. As a result, a good imaging pattern similar to that displayed in Fig. 5 has been found. The situation can be clearly found in Fig. 6, where the amplitude magnitude patterns of the total electric field along the same vertical planes as the two planes in Fig. 5 are plotted. Very bright points are still clearly observed below the lower surface of the slab.

To examine the wave propagation and image formation more clearly, we have considered the field distribution in the horizontal plane xoy at various positions around the focusing point along the z axis. The field amplitude patterns at $1.48a$, $2.26a$, and $3.04a$ from the back surface of the slab lens are displayed in Fig. 7. It is seen that the amplitude changes along the z axis. The electromagnetic waves converge first, and then diverge into far field after reaching its smallest spot at $2.26a$ away from the back surface of the slab. A close look at the data of the image spot reveals that the smallest spot size (by full size at half maximum) has a diameter of about $1.45a$ (or about 0.87λ). This shows that this inverse opal PC slab lens can achieve focusing, but not subwavelength focusing. We further determine the condition of single beam propagation. According to Ref. 25, the parallel component of the incident wave vector should fall between $-\pi/b$ and π/b. In this paper, b represents the period of the photonic crystal surface and is equal to a. We obtain that for single beam propagation the incident angles should be less than 56.01°. According to Fig. 3, the EFS exhibits a good isotropy only within about 30° and is very anisotropic beyond this incident angle. Therefore, the condition for single beam propagation can be well satisfied within the above mode space that contributes to the focusing. The fact that the focusing image spot is quite isotropic in the intensity distribution indicates that the small incident angle components of the point source play a dominant role in the focusing property of the PC slab and the influence from the high incident angle components is small.

IV. CONCLUSION

In conclusion, we have studied theoretically negative refraction of EM waves in 3D inverse opal photonic crystals and the focusing properties of flat lens made of this photonic crystal structure. The wave vector diagram is used to analyze the possibility of negative refraction, and the FDTD method is employed to simulate the field amplitude distribution. It has been found that 3D negative refraction can be achieved in the Si inverse opal photonic crystal at some certain frequency window and that the imaging functionality can be realized in a designed flat slab. The inverse opal photonic crystals can be routinely synthesized in the visible and infrared regimes, and several materials, for example, titania,[32,33] can be used as the background dielectric filling medium. The average refractive index value of titania at visible wavelengths is about 2.7, which is lower than 3.5 for silicon in our paper. High index contrast is necessary not only to achieve a wide band gap but also to have a strong plane wave component mixing of the propagating Bloch wave. In the case of weak mixing, a large number of diffracted beams appear.[25] Then, the following question arises: Can negative refraction be realized in the titania inverse opal or other inverse opals filled with different background dielectrics of lower refractive index? This remains to be answered. However, our study can help to stimulate the experimental exploitation of negative refraction and imaging in this photonic crystal at optical wavelength. This, in turn, will greatly enhance examination of other interesting physical phenomena in this photonic crystal structure.

ACKNOWLEDGMENTS

This work was supported by the National Key Basic Research Special Foundation of China through Grant No. 2004CB719804 and the National Natural Science Foundation of China through Grant Nos. 10525419 and 10404036. The support from the Supercomputing Center, CNIC, CAS is acknowledged.

*Corresponding author. Electronic address: lizy@aphy.iphy.ac.cn

[1] V. G. Veselago, Sov. Phys. Usp. **10**, 509 (1968).
[2] J. B. Pendry, A. J. Holden, W. J. Stewart, and I. Youngs, Phys. Rev. Lett. **76**, 4773 (1996).
[3] J. B. Pendry, A. J. Holden, D. J. Robbins, and W. J. Stewart, IEEE Trans. Microwave Theory Tech. **47**, 2075 (1999).
[4] J. B. Pendry, Phys. Rev. Lett. **85**, 3966 (2000).
[5] R. A. Shelby, D. R. Smith, and S. Schultz, Science **292**, 77 (2001).
[6] I. V. Lindell, S. A. Tretyakov, K. I. Nikoskinen, and S. Ilvonen, Microwave Opt. Technol. Lett. **31**, 129 (2001).
[7] L. B. Hu and S. T. Chui, Phys. Rev. B **66**, 085108 (2002).
[8] Y. Zhang, B. Fluegel, and A. Mascarenhas, Phys. Rev. Lett. **91**, 157404 (2003).
[9] Z. Feng, X. Zhang, Y. Wang, Z. Y. Li, B. Cheng, and D. Z. Zhang, Phys. Rev. Lett. **94**, 247402 (2005).
[10] M. Notomi, Phys. Rev. B **62**, 10696 (2000).
[11] C. Luo, S. G. Johnson, J. D. Joannopoulos, and J. B. Pendry, Phys. Rev. B **65**, 201104(R) (2002).
[12] Z. Y. Li and L. L. Lin, Phys. Rev. B **68**, 245110 (2003).
[13] C. Luo, S. G. Johnson, J. D. Joannopoulos, and J. B. Pendry, Phys. Rev. B **68**, 045115 (2003).

[14] S. Foteinopoulou and C. M. Soukoulis, Phys. Rev. B **67**, 235107 (2003).
[15] X. Wang, Z. F. Ren, and K. Kempa, Opt. Express **12**, 2919 (2004).
[16] X. Ao and S. He, Opt. Lett. **29**, 2542 (2004).
[17] S. Feng, Z. Y. Li, Z. F. Feng, B. Y. Cheng, and D. Z. Zhang, Phys. Rev. B **72**, 075101 (2005).
[18] S. Feng, Z. Y. Li, Z. F. Feng, K. Ren, B. Y. Cheng, and D. Z. Zhang, J. Appl. Phys. **98**, 063102 (2005).
[19] K. Ren, S. Feng, Z. F. Feng, Y. Sheng, Z. Y. Li, B. Y. Cheng, and D. Z. Zhang, Phys. Lett. A **348**, 405 (2006).
[20] E. Cubukcu, K. Aydin, E. Ozbay, S. Foteinopoulou, and C. M. Soukoulis, Nature (London) **423**, 604 (2003).
[21] E. Cubukcu, K. Aydin, E. Ozbay, S. Foteinopoulou, and C. M. Soukoulis, Phys. Rev. Lett. **91**, 207401 (2003).
[22] P. V. Parimi, W. T. Lu, P. Vodo, J. Sokoloff, J. S. Derov, and S. Sridhar, Phys. Rev. Lett. **92**, 127401 (2004).
[23] P. V. Parimi, W. T. Lu, P. Vodo, and S. Sridhar, Nature (London) **426**, 404 (2003).
[24] Z. Feng, X. Zhang, K. Ren, S. Feng, Z. Y. Li, B. Cheng, and D. Zhang, Phys. Rev. B **73**, 075118 (2006).
[25] S. Foteinopoulou and C. M. Soukoulis, Phys. Rev. B **72**, 165112 (2005).
[26] A. Berrier, M. Mulot, M. Swillo, M. Qiu, L. Thylén, A. Talneau, and S. Anand, Phys. Rev. Lett. **93**, 073902 (2004).
[27] E. Schonbrun, M. Tinker, W. Park, and J. B. Lee, IEEE Photonics Technol. Lett. **17**, 1196 (2005).
[28] C. Luo, S. G. Johnson, J. D. Joannopoulos, and J. B. Pendry, Appl. Phys. Lett. **81**, 2352 (2002).
[29] Z. Lu, J. A. Murakowski, S. Shi, C. A. Schuetz, G. J. Schneider, and D. W. Prather, Phys. Rev. Lett. **95**, 153901 (2005).
[30] S. Yang, J. H. Page, Z. Liu, M. L. Cowan, C. T. Chan, and P. Sheng, Phys. Rev. Lett. **93**, 024301 (2004).
[31] C. Monzon, P. Loschialpo, D. Smith, F. Rachford, P. Moore, and D. W. Forester, Phys. Rev. Lett. **96**, 207402 (2006).
[32] J. E. G. J. Wijnhoven and W. L. Vos, Science **281**, 802 (1998).
[33] G. Subramania, K. Constant, R. Biswas, M. M. Sigalas, and K. M. Ho, Appl. Phys. Lett. **74**, 3933 (1999).
[34] Y. Vlasov, X. Bo, J. C. Sturm, and D. J. Norris, Nature (London) **414**, 289 (2001).
[35] P. G. Ni, B. Y. Cheng, and D. Z. Zhang, Appl. Phys. Lett. **80**, 1879 (2002).
[36] K. M. Ho, C. T. Chan, and C. M. Soukoulis, Phys. Rev. Lett. **65**, 3152 (1990).
[37] Z. Y. Li, J. Wang, and B. Y. Gu, Phys. Rev. B **58**, 3721 (1998).
[38] A. Taflove, *Computation Electromagnetics: The Finite-Difference Time-Domain* (Artech House, Boston, 1995).
[39] J. P. Berenger, J. Comput. Phys. **114**, 185 (1994).
[40] R. Moussa, Th. Koschny, and C. M. Soukoulis, Phys. Rev. B **74**, 115111 (2006).